Assessment of Fatigue Crack Initiation Behaviour in Ti-6Al-4V Alloy Using a Coarsened Surrogate Model

Toda, Hiroyuki
Department of Mechanical Engineering, Kyushu University

Feng, Shuo
Department of Mechanical Engineering, Kyushu University

Fujihara, Hiro
Department of Mechanical Engineering, Kyushu University

Tubei, Valary
Department of Mechanical Engineering, Kyushu University

他

出版情報：MATERIALS TRANSACTIONS. 66 (8), pp.973-981, 2025-08-01. 日本金属学会
バージョン：

Materials Transactions, Vol. 66, No. 8 (2025) pp. 973 to 981

Assessment of Fatigue Crack Initiation Behaviour in Ti-6Al-4V Alloy Using a Coarsened Surrogate Model

Hiroyuki Toda[1,*], Shuo Feng[1], Hiro Fujihara[1], Valary Tubei[1], Akihisa Takeuchi[2] and Masayuki Uesugi[2]

[1]*Department of Mechanical Engineering, Kyushu University, Fukuoka 819-0395, Japan*
[2]*Japan Synchrotron Radiation Research Institute, Sayo-gun, Hyogo 679-5198, Japan*

The microstructure and fatigue crack initiation process of Ti-6Al-4V alloys were measured using a multimodal technique combining synchrotron X-ray microtomography and electron backscatter diffraction (EBSD) serial sectioning techniques. Various microstructural design variables were generated to describe the shape, size and crystallographic information of the polycrystalline microstructure that is the fatigue crack initiation point. The microstructural information was coarsened based on the similarity between the design variables and their correlation with fatigue crack initiation. An objective function describing the resistance to fatigue crack initiation was also established. By combining these variables, the relationship between the microstructural information and fatigue crack initiation resistance was described by a metamodel in the form of a multidimensional response surface using a support vector machine. A limited number of design variables with a high correlation with transgranular and intergranular fatigue cracking were identified, and the optimum or weakest microstructural patterns for fatigue crack initiation were quantitatively represented. This approach is expected to allow much more efficient microstructure control to enhance the fatigue crack initiation resistance than has previously been possible with the conventional surface-based approach. [doi:10.2320/matertrans.MT-L2025002]

(Received February 21, 2025; Accepted April 11, 2025; Published May 23, 2025)

Keywords: *titanium, fatigue, crack initiation, 3D observation, statistical analysis, optimisation*

1. Introduction

In general, detection of fatigue cracks with high accuracy immediately after their initiation is technically difficult. In addition, no current theoretical model can accurately predict crack initiation [1]. Therefore, the determination of fatigue crack initiation is usually accompanied by some ambiguity. In other words, there are no agreed-upon criteria at what size, from lattice defects to macroscopic cracks, fatigue crack initiation is judged to have occurred. Therefore, in many cases, the propagation process of short fatigue cracks is added to fatigue crack initiation to some extent, and fatigue crack initiation is judged to have occurred when the crack length reaches a relatively large specific dimension. Therefore, even when the fatigue life is predicted, the fatigue crack initiation life is not considered but is evaluated via fatigue crack propagation analysis assuming an initial crack [2].

In terms of the actual fatigue crack initiation process, inclusions and pores can be the initiation sites, as in aluminium alloys [3]. In practical alloys, fatigue cracks tend to form in persistent slip bands at low stress amplitudes and at grain boundaries at high stress amplitudes [4]. In persistent slip bands, fatigue cracks are initiated by the intrusion-extrusion mechanism, particularly on slip planes oriented in an oblique direction (e.g., 45°) to the stress axis [4]. It is also known that different forms of fatigue crack initiation, such as in persistent slip bands and at grain boundaries, inclusions and pores, cause the fatigue life to vary [5]. In addition, the formation of compressive residual stresses and hardened microstructures in the surface layer by shot peening, etc. can delay fatigue crack initiation and lead to improved fatigue life [6]. Therefore, control of the microstructure is important to increase the resistance to fatigue crack initiation after the relationships between the microstructure and fatigue crack initiation mechanisms are understood. Of these mechanisms, fatigue crack initiation at inclusions and pores can be suppressed by relatively simple microstructure control, such as refining the inclusions and pores and/or reducing their number density. Control of the remaining persistent slip bands and grain boundaries is less straightforward, as they are related to various aspects of the polycrystalline microstructure, such as the crystal orientation and grain size and shape.

The effects of the grain size [7], Schmid factors related to the crystal orientation [8] and grain boundary characteristics [9] on fatigue crack initiation have been investigated via surface observation. Prediction of S-N curves based on such information has been attempted [10]. Image-based crystal-plasticity finite element analysis has also been used to understand the experimental results [11]. Understanding the influence of polycrystalline microstructures is particularly important for titanium alloys, in which the slip system is limited compared to steel and aluminium. For example, Liu *et al.* investigated the fatigue crack initiation behaviour in titanium alloys with a bimodal microstructure and studied the relationships of crack initiation at basal planes with the Schmid factor and the angle between the loading axis and the c-axis [12]. However, all previous experimental and analytical evaluations have been two-dimensional, relying on surface information, and the formation of slip zones, etc. has only been qualitatively interpreted [8].

The authors have proposed a statistical analysis method in which various morphological and crystallographic factors describing microstructures are taken as microstructural design variables, and their relationships with an objective function describing deformation, damage and fracture are described by a metamodel [13]. This allows a limited number of design variables with a strong correlation with the objective function to be extracted and the values of the design variables describing the optimum or weakest microstructure to be obtained, thus allowing efficient design of microstructures. In a specific method, the values of the

*Corresponding author, E-mail: toda@mech.kyushu-u.ac.jp

various design variables are directly measured via high-resolution 3D imaging, and if necessary, 3D image-based simulation is used to predict the values of the target variables for analysis. The influence of the particles dispersed and polycrystalline microstructure of aluminium on the material strength and hydrogen embrittlement was analysed using this method [14–17]. In the present study, this method was applied to the problem of fatigue crack initiation in titanium alloys, with the aim of quantitatively presenting a microstructure with superior resistance to fatigue crack initiation.

2. Experimental and Analytical Methods

2.1 *In-situ* observation of fatigue crack initiation

The material analysed was the same Ti-6Al-4V alloy as that previously reported [18, 19]. The received material was hot rolled at 800°C and annealed at 900°C for 96 hours. The specimens have a bimodal microstructure consisting of the α phase and α + β lamellar phase. The volume fraction of the α + β lamellar phase is 35%, and the average grain size of the α phase is approximately 20 μm. The plate specimens were electropolished, and seven fatigue specimens with the same geometry (cross-section of 500 μm × 500 μm) as that previously reported were prepared [18, 19].

Based on the S–N diagram in Fig. 1, the maximum stress was set to 700 MPa or 750 MPa, corresponding to approximately 80% or 86% of the 0.2% proof stress of the material, and a sinusoidal loading waveform with a stress ratio of $R = 0.1$ and a frequency of 15 Hz was applied. After 20,000 loading cycles were applied to all specimens, crack initiation was observed in 3D via projection X-ray computed tomography (CT). When cracks were not observed, the number of cycles was increased by 5000 each time to see if crack initiation occurred. During the observation, a load equal to 50% of the maximum fatigue stress was applied to facilitate crack detection. The observations were performed at the high-resolution imaging beamline BL20XU at the synchrotron radiation facility SPring-8. The X-ray energy used was 30 keV, and the exposure time was 50 ms. 3D images with a voxel size of 0.49 μm^3 were reconstructed from 1800 projected 2D images acquired with a camera length of 53 mm. The effective spatial resolution was approximately 1 μm, which is the theoretical spatial resolution of projected X-ray CT.

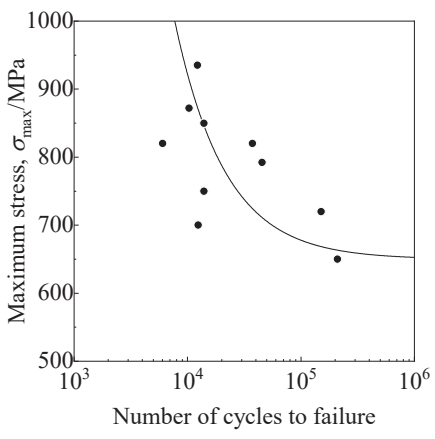

Fig. 1 S–N diagram obtained at R = 0.1 and a frequency of 15 Hz.

Initially, the α and α + β phases were separated by a segmentation process, followed by Watershed processing to estimate the locations of grain boundaries. After fatigue tests, the specimens were not fractured and the electron backscatter diffraction (EBSD) serial sectioning method was used to obtain more accurate information on the locations and morphologies of the grain boundaries to correct the post-watershed images. The slice thickness of the 3D polycrystalline microstructure images obtained by serial sectioning was 5 μm, and the step size of the EBSD measurements was 0.7 μm.

2.2 Statistical analysis of fatigue crack initiation

To correlate the individual grain and grain boundary properties obtained by 3D imaging with the presence or absence of, and susceptibility to, fatigue crack initiation, the polycrystalline microstructure in relation to fatigue crack initiation was quantitatively evaluated with numerous design variables. When fatigue crack initiation occurred within the grains, the initiation locations were restricted to within the α phase. Therefore, 22 design variables describing the geometric and crystallographic features of the α phase grains were prepared, as shown in Table 1. In contrast, when fatigue cracks initiated at the grain boundaries, it was observed in the specimens that the cracks initiated at a grain boundary between two α phase grains. Therefore, 20 design variables describing the geometric and crystallographic information of the two α phase grain pairs were prepared, as also shown in Table 1. Coarsening was then performed using principal component analysis and global sensitivity analysis, taking into account the similarity between the design variables and their correlation with the objective function. Details of the methodology can be found in a previous report [13].

The presence and ease of fatigue crack initiation was quantified and used as the objective function, I, to be optimised. Specifically, the following equation was used.

$$I = \left(\frac{700}{\sigma}\right)\left(\frac{\log N_{min}}{\log N}\right) \tag{1}$$

where σ is the maximum stress under fatigue loading, N is the number of the cycle at which fatigue crack initiation was first observed, and $N_{\min}$ is the minimum value of N in the grains where fatigue cracks were observed. In α phase grains where no fatigue crack initiation was observed, $I = 0$ was assumed. All the design variables and the objective function were dimensionless so that the upper 5% and lower 5% of the points in the distribution of the values of each design variable and the objective function were between 0 and 1 [13].

The relationship between the α phase polycrystalline microstructure and fatigue crack initiation resistance was modelled by meta-modelling using the few design variables that were ultimately selected. Because the amount of fatigue crack initiation data in this study is limited, a support vector machine was used, which could accurately represent the output data from a limited amount of input data. After the optimum values of the selected design variables were determined (i.e., the values that can minimise the objective variable), the relationship between any two design variables

Table 1 Design variables for transgranular and intergranular fatigue crack initiation.

Transgranular crack initiation		
Category	Variables	Remark
I. Grain Shape	$f_1 = W_y / L_x$	Length to width ratio in the *x*-*y* plane
	$f_2 = W_y / T_z$	Shape elongation in the loading direction (*y*-*z* plane)
	$f_3 = L_x / T_z$	Shape elongation perpendicular to the loading direction (*x*-*z* plane)
	$f_4 = 6\sqrt{\pi}\frac{V}{\sqrt{S^3}}$	Shape deviation from a sphere expressed with *V* and *S*
	$f_5 = 48\pi^2\frac{V}{M^3}$	Shape deviation from a sphere expressed with *V* and *M*
	$f_6 = 4\pi\frac{S}{M^2}$	Shape deviation from a sphere expressed with *S* and *M*
	$f_7 = 216\frac{V^2}{S^3}$	Shape deviation from a cube expressed with *V* and *S*
	$f_8 = 288\frac{V}{M^3}$	Shape deviation from a cube expressed with *V* and *M*
	$f_9 = 16\frac{S}{M^2}$	Shape deviation from a cube with *S* and *M*
	$f_{10} = \frac{\pi G e^3}{216V}$	Elongation index
	M	Integral of mean curvature
II. Grain size	L_x	Length in the *x* direction
	W_y	Width in the *y* direction
	T_z	Thickness in the *z* direction
	A	Surface area
	V	Volume
	D	Diameter
	G	Geodesic distance on grain surface
III. Orientation	*BS*	Basal Schmid factor
	PS	Prismatic Schmid factor
	PyS	Pyramidal Schmid factor
	S	Maximum Schmid factor among *BS, PS* and *PyS*
Intergranular crack initiation		
I. Shape	F_1, F_2, F_3	Ratio of aspect ratios of grains expressed with f_1, f_2 and f_3
	F_4, F_5, F_6	Ratio of spherical deviations of grains expressed with f_4, f_5 and f_6
	F_7, F_8, F_9	Ratio of cubic deviations of grains expressed with f_7, f_8 and f_9
	F_{10}	Ratio of elongation indices
	R_M	Ratio of integral of mean curvature
II. Grain size	R_A	Ratio of surface area
	R_V	Ratio of grain volume
	R_{dia}	Ratio of diameter
	R_G	Ratio of geodesic distance
III. Orientation	R_{BS}	Ratio of basal Schmid factor values
	R_{PS}	Ratio of prismatic Schmid factor values
	R_{PyS}	Ratio of pyramidal Schmid factor values
	R_S	Ratio of maximum Schmid factor values
	θ_{Mis}	Misorientation angle between neighbouring grains

and the objective function was visualised using response surface methodology. In this case, the design variables not used to construct the response surface were held constant at their respective optimum values. The details of the meta-modelling process are also described in a previous paper [13].

3. Results and Discussions

3.1 Fatigue test results

Figure 2 shows 3D X-ray CT images of specimen gauge sections. The titanium matrix and its microstructure are obscured, and only the fatigue cracks are shown. A total of 13 fatigue cracks were observed in 5 specimens. In specimens B and G, multiple fatigue crack initiation was observed after 20,000 cycles. In contrast, the initiation of only one fatigue crack was observed in specimens A and C up to 35,000 cycles. The geometric and crystallographic information of the α phase grains or grain boundaries at which three identified transgranular cracks and six intergranular cracks were generated was obtained by EBSD serial sectioning. Additionally, 257 randomly selected α phase grains in which fatigue cracks did not develop were also selected for analysis.

3.2 Coarsening

Figure 3 and Fig. 4 summarise the coarsening results for transgranular and intergranular cracks. First, in terms of the removal of similar design variables, combinations for which the angle between the eigenvectors of the two design variables was less than 5° (Fig. 3(a) and (b)) were extracted by principal component analysis, and the design variables with smaller contributions were removed. In addition, a global sensitivity analysis was applied to the remaining design variables, and they were ordered by the correlation coefficients, as shown in Fig. 4(a) and (b). For transgranular cracking, the design variables correlated with fatigue crack initiation were all related to the grain shape. There was also a weak correlation with the crystallographic orientation and little correlation with the grain size. For transgranular cracking, the metamodels with high correlation coefficients, i.e., M (integral of the mean curvature of the grain surface), f_6 (spherical deviation of a grain), f_1 (aspect ratio of a grain in the x-y plane), f_3 (aspect ratio of a grain in the x-z plane), f_7 (cubic deviation of a grain) and BS (Schmid factor for basal slip), were selected to generate a metamodel.

In contrast, for intergranular cracks, there was a strong correlation with the crystallographic orientation and a weak correlation with the grain shape and size. The correlation coefficients for RS (maximum Schmid factor ratio of two

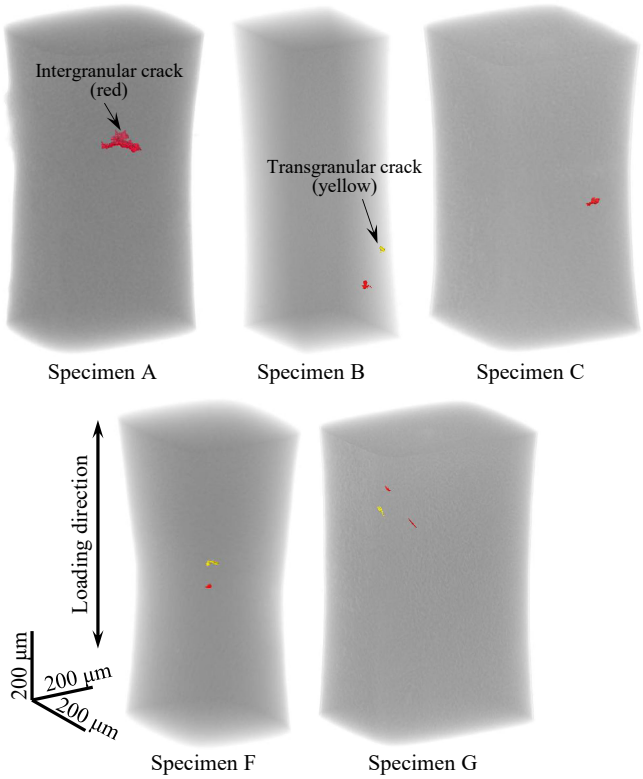

Fig. 2 3D morphologies of fatigue cracks immediately after their initiation. X-ray CT images were volume rendered to show the locations and 3D morphologies of the fatigue cracks in each specimen. (online color)

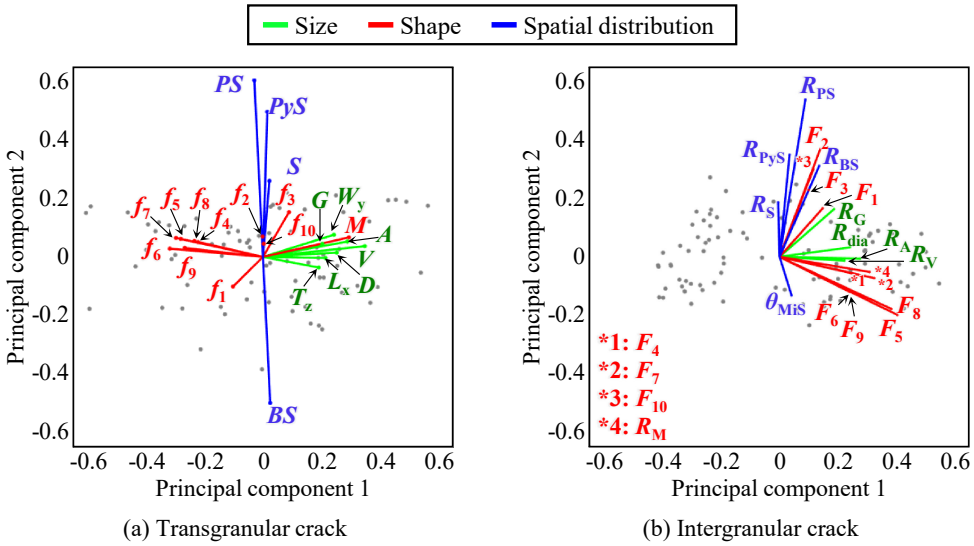

(a) Transgranular crack (b) Intergranular crack

Fig. 3 Results of the first-stage coarsening process for design variables using principal component analysis for both (a) transgranular and (b) intergranular fatigue crack initiation. (online color)

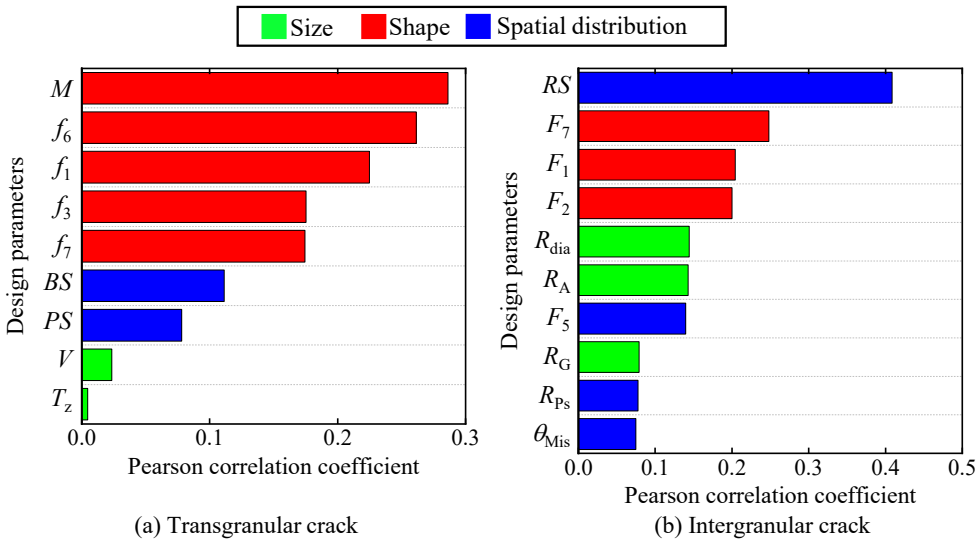

Fig. 4 Results of the second-stage coarsening process for design variables using global sensitivity analysis for both (a) transgranular and (b) intergranular fatigue crack initiation. (online color)

grains across a grain boundary), F_7 (spherical deviation ratio of two grains across a grain boundary, defined using the volume and surface area), F_1 (ratio of the aspect ratios in the x-y plane of two grains across a grain boundary), F_2 (ratio of the aspect ratios in the y-z plane of two grains across a grain boundary), R_{dia} (ratio of the diameters of two grains across a grain boundary), R_A (ratio of the surface areas of two grains across a grain boundary) and F_5 (ratio of the spherical deviations of two grains across a grain boundary, defined using the volume and mean curvature) were selected to create a metamodel.

3.3 Response surfaces between microstructural features and fatigue crack initiation resistance

Figure 5 illustrates the response surfaces that were created using the combination of design variables that exhibited the most evident dependence on the objective function and were straightforward to comprehend in terms of their physical meaning, out of the many combinations of design variables that were ultimately retained. The black data points in the graphs represent the design variable values for α phase grains in which cracks formed, while the white data points represent the design variable values for α phase grains in which cracks did not form. The yellow points indicate the microstructure for which the objective function predicted by the metamodel is the lowest (optimum microstructure). Figure 6 shows the projection of the response surface curves onto the design spaces to facilitate location in the design spaces of the predicted optimum microstructures and the damaged microstructures in the fatigue test.

(1) Transgranular cracking

First, attention is given to the response surfaces between the resistance to transgranular crack initiation and f_1/f_6 in Fig. 5(a) and Fig. 6(a). The weakest point for fatigue crack initiation are $f_1 = 0$ and $f_6 = 0$ after normalisation, corresponding to a flattened oblong shape. The optimum point are $f_1 = 1$ and $f_6 = 1$ after normalisation, corresponding to flatter and rather oval grains. This is consistent with the fact that, in general, α phase grains flattened and elongated in the loading direction have their internal stresses easily increased and have a low resistance to fatigue crack initiation. Next, the Schmid factors for basal slip in Fig. 5(b) and Fig. 6(b), also for transgranular fatigue cracks, show that the weakest point occurs at $BS = 1$ and the optimum point occurs at $BS = 0.44$, but the dependence is much lower. This corresponds to the low correlation coefficient of the Schmid factor for basal slip in Fig. 4.

(2) Intergranular cracking

The dependence of the objective function for intergranular crack initiation on R_S, F_7, F_1 and R_{dia} is shown in Fig. 5(c)–(d) and Fig. 6(c)–(d). In Fig. 5(c) and Fig. 6(c), the weakest point correspond to $F_7 = 1$ and $R_S = 0$. This indicates a case in which the shapes of the two α phase grains across a grain boundary are similar in terms of spherical deviation and in which the maximum Schmid factors of the two α phase grains across the grain boundary are extremely different. This corresponds to the case in which the Schmid factor of only one grain is practically large in the experimental data. In contrast, the optimum crystallographic microstructure in terms of intergranular fatigue crack initiation corresponds to $F_7 = 0.39$ and $R_S = 0$, i.e., when the grain shapes, quantified by the spherical deviation, for the two α phase grains across a grain boundary are different and when the difference in the Schmid factors of the two α phase grains is large. The response surface has a larger slope near the optimum point, whereas the areas of the F_7 and R_S values near the weakest point are larger. This suggests that precise microstructural control is required to improve the fatigue crack initiation resistance. In Fig. 5(d) and Fig. 6(d), the dependence on R_{dia} is relatively small, which corresponds to the relatively low correlation coefficient of R_{dia} for basal slip in Fig. 4. The weakest point corresponds to $R_{dia} = 1$ (the two α phase grains across a grain boundary are of similar sizes), and the optimum point corresponds to $R_{dia} = 0$ (the difference in the size between the two grains across a grain boundary is the maximum). Figures 5(e) and 6(e) show that the dependence on F_1 is also relatively small compared to that on F_7. The weakest point corresponds to $F_1 = 0.67$, and the

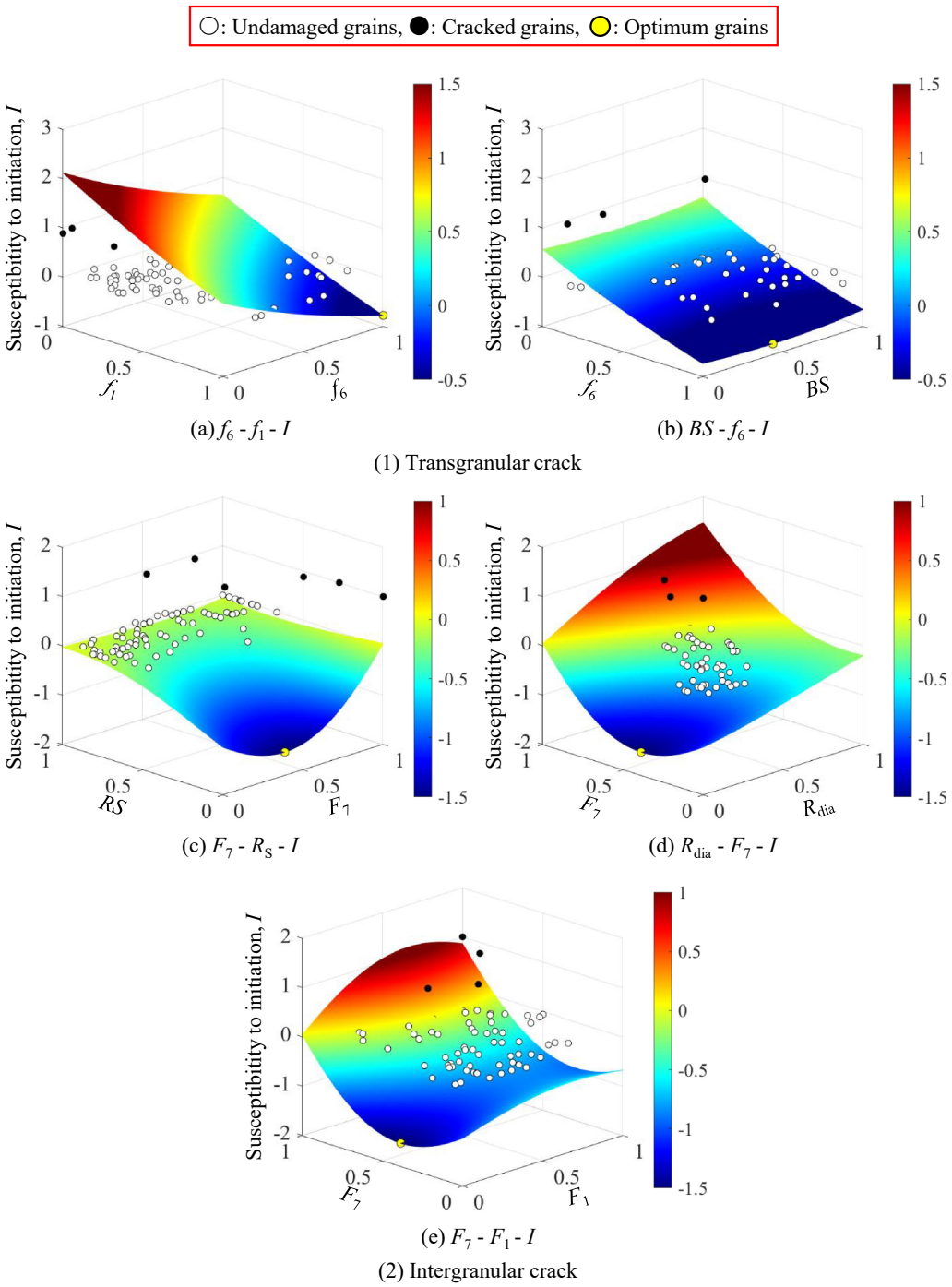

Fig. 5 3D response surface curves for (1) transgranular and (2) intergranular fatigue cracks. A representative combination of a couple of selected design variables and the objective function (i.e., the susceptibility to fatigue crack initiation) are shown in each figure. The levels of the objective function values of the response surface curves are expressed as colour contours. (online color)

optimum point corresponds to $F_1 = 0$. Thus, grains with similar aspect ratios are more prone to fatigue cracking.

3.4 Interpretation of the findings and their industrial applications

To visually and intuitively understand the statistical analysis results, the α phase grains and grain pairs sandwiching grain boundaries closest to the weakest and optimal microstructures predicted by the metamodels in Fig. 5(a)–(d) were extracted and are shown as 3D representations of X-ray CT images in Fig. 7. Intuitively, Fig. 7(a)–(b) shows that transgranular fatigue crack initiation is more likely to occur in α phase grains with retarded recrystallisation and coarse and distorted shapes that are elongated in the loading direction. The complexity of the grain shape promotes crack initiation due to strain localisation. Coarse α phase grains also initiate slip deformation earlier, forming larger slip displacements and facilitating crack initiation. Conversely, relatively fine α phase grains that have been suppressed in growth due to the pinning effect of grain boundary particles or immediately after the onset of recrystallisation can be said to have a greater resistance to the

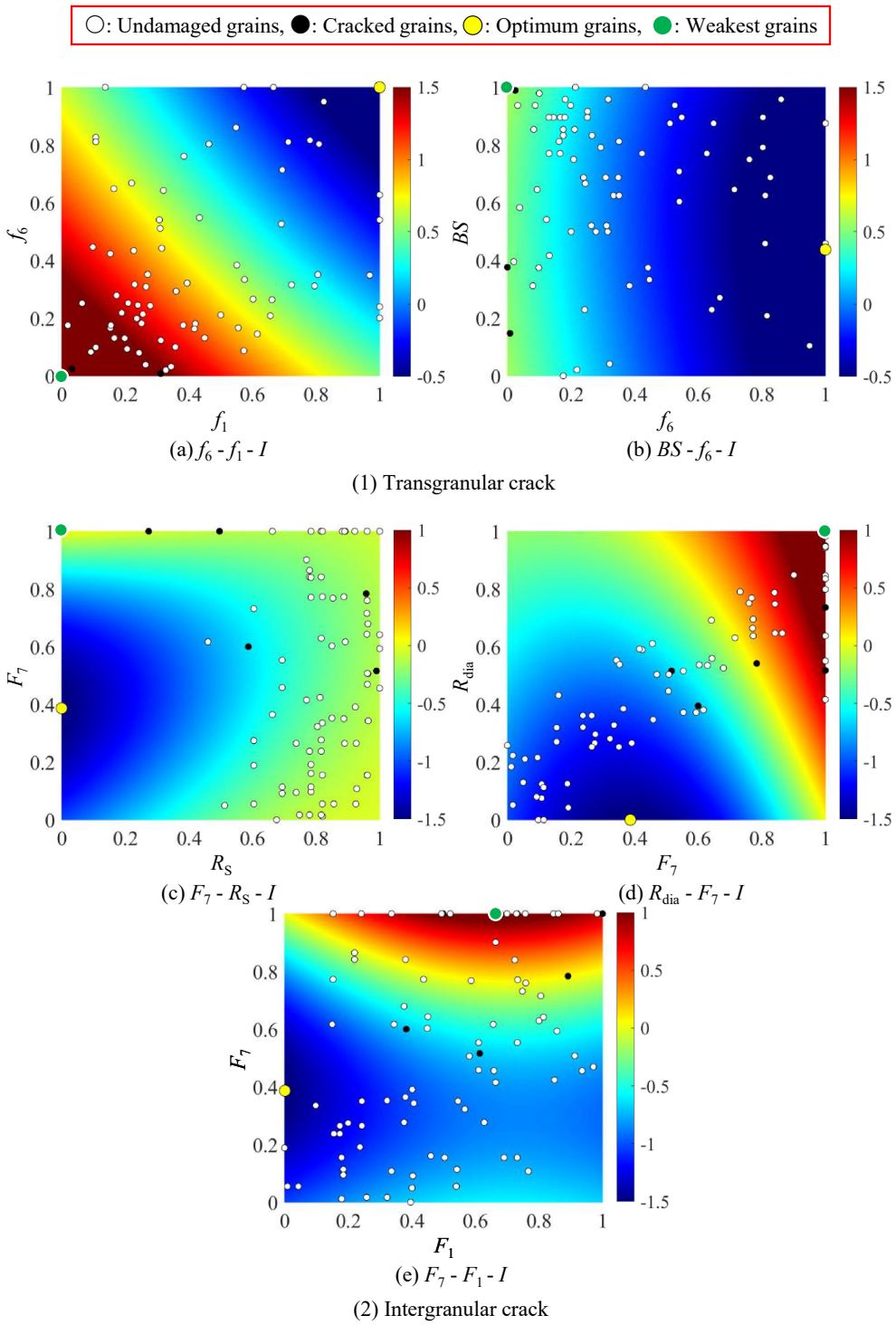

Fig. 6 3D response surface curves projected onto the design spaces for (1) transgranular and (2) intergranular fatigue cracks. A combination identical to that in Fig. 2 of a couple of selected design variables and the objective function are shown in each figure. The levels of the objective function values of the response surface curves are expressed as colour contours. (online color)

initiation of fatigue cracks. The reason why grain size is not included in the extracted design variables is that there is originally a high correlation between the grain shape and size, which is described by the shape variables with a greater contribution in the metamodel. In fact, the equations for design variables f_1–f_{10} include some size-related design variables. The occurrence of transgranular fatigue cracks was unexpectedly found to be less sensitive to the crystallographic orientation. This suggests that the orientation of the basal planes alone does not dictate fatigue crack initiation, as fatigue crack initiation may also occur on the pyramidal and prismatic planes.

Additionally, regarding the occurrence of intergranular fatigue cracks, the probability increases when there are adjacent α phase grains of similar size, shape and Schmid factor, as shown in Fig. 7(c)–(d). In particular, if the Schmid factors of the α phase grain pair are both high and if the two grains across a grain boundary both undergo early principal

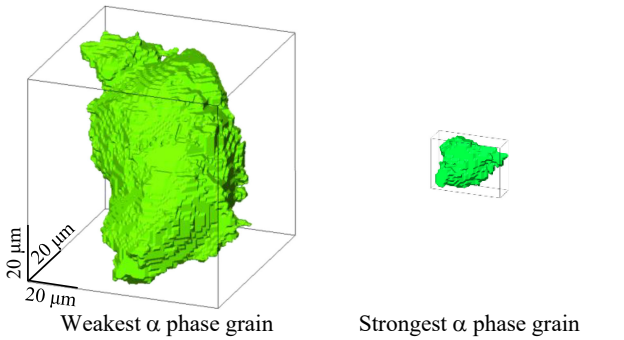

Weakest α phase grain Strongest α phase grain

(a) Optimisation in f_6 - f_1 - I space for transgranular initiation

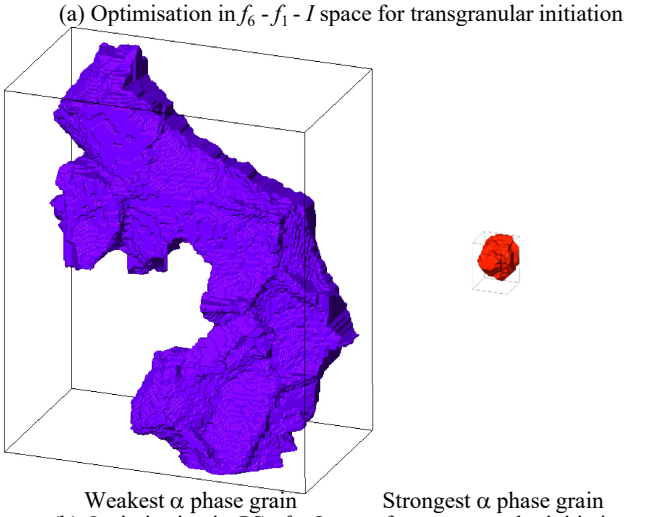

Weakest α phase grain Strongest α phase grain

(b) Optimisation in BS - f_6 - I space for transgranular initiation

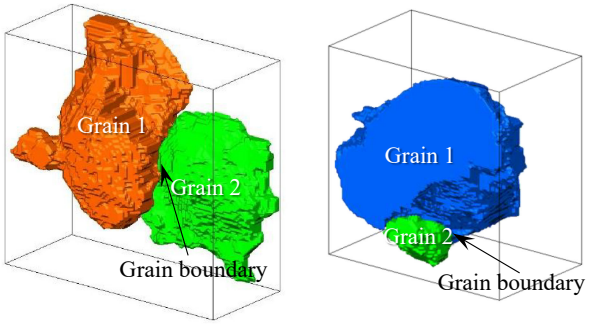

Weakest grain pair Strongest grain pair

(c) Optimisation in $F_7 - R_S$ - I space for intergranular initiation

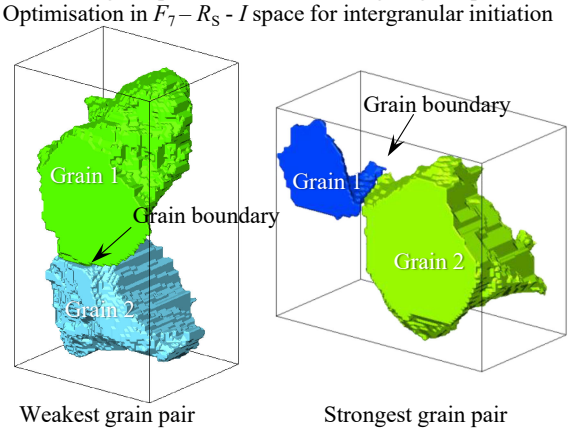

Weakest grain pair Strongest grain pair

(d) Optimisation in $R_{dia} - F_7$ - I space for intergranular initiation

Fig. 7 The actually observed grains and grain pairs closest to the weakest and optimal microstructures predicted by the metamodels in Fig. 3(a)–(d) were extracted and are shown as 3D representations of X-ray CT images. (online color)

slip, then the mismatch in deformation at the grain boundary will be large because an orientation difference in the principal slip system will statistically appear. This is thought to be an important driving force for intergranular fatigue crack initiation.

The above findings are further discussed in relation to the actual microstructural control processes of metallic materials. Transgranular fatigue cracking is more likely to occur in α phase grains with retarded recrystallisation and coarse and distorted geometries that are elongated in the loading direction. The recrystallisation rate is influenced by alloying elements, temperature and time. Some recrystallisation is necessary, but too much coarsening after recrystallisation can actually reduce the resistance to transgranular fatigue cracking, especially if there are discrete particles that can confine the recrystallisation. In terms of intergranular fatigue cracking, a bimodal polycrystalline microstructure with moderately advanced recrystallisation is preferable. Searching for the optimum bimodal microstructure while being aware of any reduction in the resistance to transgranular fatigue cracking is therefore important.

The evaluation of the grain size and sphericity based on 2D morphological information of cross sections obtained using scanning electron microscopy or other means has been the basis of conventional microstructure control. In this study, 3D observations of the polycrystalline microstructure were carried out, and when transgranular fatigue crack initiation was observed, the design variables M, f_6, f_1, f_3, f_7 and BS, which are highly correlated with the crack initiation resistance, were measured. Control of the 3D geometry of the crystal grains was found to be particularly important. In contrast, R_S, F_7, F_1, F_2, R_{dia}, R_A and F_5 are important when intergranular fatigue crack initiation is observed, and control of the distributions of the grain shape and grain orientation by controlling the recrystallisation process is useful. The combination of 3D observation and 3D quantitative evaluation of the crystallographic orientation and grain properties is expected to enable more efficient suppression of fatigue crack initiation than ever before. In this study, X-ray CT using synchrotron radiation was used for this purpose. This technique is difficult to use in routine material design and evaluation processes. Recently, however, 3D morphological and crystallographic information of grains has been obtained at the laboratory level using EBSD serial sectioning and diffraction contrast tomography (DCT) methods [20]. The microstructure control described above is expected to become more realistic through the use of these methods.

4. Conclusion

In this study, the microstructure and fatigue crack initiation process of a Ti-6Al-4V alloy were measured using a multimodal approach combining synchrotron X-ray CT and EBSD serial sectioning. A variety of microstructural design variables describing the shape, size and crystallographic information of the polycrystalline microstructure were generated, and a limited number of design variables that strongly correlated with fatigue crack initiation were extracted. A statistical analysis method was then used to

describe the relationship between these variables and the objective function describing the fatigue crack initiation resistance in a metamodel. The design variables with high correlations were identified for both transgranular and intergranular fatigue cracking, and the values of the design variables describing the optimum or weakest microstructure were obtained to quantitatively represent the microstructure with excellent resistance to fatigue crack initiation. This approach is expected to provide much more efficient microstructure control than conventional microstructure control.

Acknowledgments

The synchrotron experiments were performed with the approval of JASRI under proposal numbers 2022B1158, 2023A1005, and 2023B1011. This work was supported by JSPS KAKENHI Grant Nos. JP17H01328, JP21H04624 and 23K13564 the Japan Science and Technology Agency (JST) through the Core Research for Evolutional Science and Technology (CREST) project (Grant No. JPMJCR1995), and the Light Metal Educational Foundation.

REFERENCES

[1] F. Scoetens, I.J. Van Straalen and O.D. Dijkstra: European research on fatigue of aluminium structures, Proc. Sixth Int. Conf. Alum., (1995) pp. 53–64.
[2] J.A. Hall: Fatigue crack initiation in alpha-beta titanium alloys, Int. J. Fatigue **19** (1997) 23–37.
[3] K. Tanaka and T. Mura: A theory of fatigue crack initiation at inclusions, Metall. Trans. A **13** (1982) 117–123.
[4] S. Suresh: *Fatigue of Materials*, (Cambridge University Press, 1998).
[5] K.S. Ravi Chandran and S.K. Jha: Duality of the S-N fatigue curve caused by competing failure modes in a titanium alloy and the role of Poisson defect statistics, Acta Mater. **53** (2005) 1867–1881.
[6] S. Roy, J.W. Fisher and B.T. Yen: Fatigue resistance of welded details enhanced by ultrasonic impact treatment (UIT), Int. J. Fatigue **25** (2003) 1239–1247.
[7] P. Lukáš and L. Kunz: Effect of grain size on the high cycle fatigue behaviour of polycrystalline copper, Mater. Sci. Eng. **85** (1987) 67–75.
[8] J.E. Bozek *et al.*: A geometric approach to modeling microstructurally small fatigue crack formation: I. Probabilistic simulation of constituent particle cracking in AA 7075-T651, Model. Simul. Mater. Sci. Eng. **16** (2008) 065007.
[9] L.C. Lim: Surface intergranular cracking in large strain fatigue, Acta Metall. **35** (1987) 1653–1662.
[10] M.D. Sangid, H.J. Maier and H. Sehitogl: An energy-based microstructure model to account for fatigue scatter in polycrystals, J. Mechan. Phys. Solids **59** (2011) 595–609.
[11] J. Thomas, M. Groeber and S. Ghosh: Image-based crystal plasticity FE framework for microstructure dependent properties of Ti–6Al–4V alloys, Mater. Sci. Eng. A **553** (2012) 164–175.
[12] C. Liu, R. Thomas, J. Quinta da Fonseca and M. Preuss: Early slip activity and fatigue crack initiation of a near alpha titanium alloy, MATEC Web Conf. **321** (2020) 11040.
[13] H. Toda, H. Li, R. Batres, K. Hirayama and H. Fujihara: Surrogate-based optimization of microstructural features of structural materials, Acta Mater. **257** (2023) 119188.
[14] H. Toda, K. Hirayama, S. Yamaguchi, H. Fujihara, R. Higa, K. Shimizu, A. Takeuchi and M. Uesugi: Dominant Factors Controlling the Initiation of Hydrogen Embrittlement in Al–Zn–Mg Alloy, Mater. Trans. **64** (2023) 2729–2738.
[15] H. Toda, H. Fujihara, K. Hirayama, K. Shimizu, Y. Wang, S. Bhupendra, J. Tang, A. Takeuchi and M. Uesugi: Hydrogen Induced Debonding of Mg_2Si Particle/Aluminum Interface in Al-Mg-Si Alloy, Mater. Trans. **65** (2024) 763–772.
[16] H. Toda, K. Hirayama, H. Li, R. Batres, S. Dowon and H. Fujihara: Maximising mechanical properties of aluminium alloys by micro-structural optimisation using a coarsened surrogate model, Comput. Mater. Sci. **243** (2024) 113115.
[17] H. Toda, Y. Fukuda, H. Li, K. Hirayama, H. Fujihara, K. Shimizu, Y. Wang, J. Tang, A. Takeuchi and M. Uesugi: Surrogate model-based assessment of particle damage behaviour of Al Zn Mg alloy, Acta Mater. **281** (2024) 120391.
[18] M. Hassanipour, S. Watanabe, K. Hirayama, H. Toda, K. Uesugi and A. Takeuchi: Short crack growth behavior and its transitional interaction with 3D microstructure in Ti-6Al-4V, Mater. Sci. Eng. A **738** (2018) 229–237.
[19] M. Hassanipour, S. Watanabe, K. Hirayama, H. Li, H. Toda, K. Uesugi and A. Takeuchi: Assessment of predominant microstructural features controlling 3D short crack growth behavior via a surrogate approach in Ti-6Al-4V, Mater. Sci. Eng. A **751** (2019) 351–362.
[20] H. Toda: *X-Ray CT: Hardware and Software Techniques*, (Springer Nature, Singapore, 2021).